Mechanisms of transport enhancement for self-propelled nanoswimmers in a porous matrix

Haichao Wu[a], Benjamin Greydanus[a], and Daniel K. Schwartz[a,1]

[a]Department of Chemical and Biological Engineering, University of Colorado Boulder, Boulder, CO 80309

Edited by Michael P. Brenner, Harvard University, Cambridge, MA, and accepted by Editorial Board Member Joanna Aizenberg May 23, 2021 (received for review January 29, 2021)

Micro/nanoswimmers convert diverse energy sources into directional movement, demonstrating significant promise for biomedical and environmental applications, many of which involve complex, tortuous, or crowded environments. Here, we investigated the transport behavior of self-propelled catalytic Janus particles in a complex interconnected porous void space, where the rate-determining step involves the escape from a cavity and translocation through holes to adjacent cavities. Surprisingly, self-propelled nanoswimmers escaped from cavities more than 20× faster than passive (Brownian) particles, despite the fact that the mobility of nanoswimmers was less than 2× greater than that of passive particles in unconfined bulk liquid. Combining experimental measurements, Monte Carlo simulations, and theoretical calculations, we found that the escape of nanoswimmers was enhanced by nuanced secondary effects of self-propulsion which were amplified in confined environments. In particular, active escape was facilitated by anomalously rapid confined short-time mobility, highly efficient surface-mediated searching for holes, and the effective abolition of entropic and/or electrostatic barriers at the exit hole regions by propulsion forces. The latter mechanism converted the escape process from barrier-limited to search-limited. These findings provide general and important insights into micro/nanoswimmer mobility in complex environments.

nanoswimmers | three-dimensional tracking | porous materials | self-propulsion | cavity escape

Micro- and nanoscale robots are capable of taking energy from their environment and converting it to directional motion. A variety of micro/nanoswimmers based on different actuation principles have been developed recently, including chemically powered colloidal particles (1, 2), magnetic swimmers (3, 4), photocatalytic nanomotors (5, 6), and acoustic microrods (7, 8). They have attracted considerable interest because of their potential biomedical and environmental applications, such as biomedical diagnosis (9, 10), drug delivery (11, 12), and environmental remediation (13, 14). However, these applied scenarios often require efficient motion of micro/nanoswimmers within complex tortuous, crowded, and interconnected environments, like microfluidic devices and biological tissues, and the current understanding of nanoswimmer transport remains incomplete in this regard.

The transport of micro/nanoswimmers in confined environments is intrinsically complex due to the strong coupling of translational and orientational motion with interfaces, among other effects. Moreover, their motion is influenced by both thermal fluctuations and self-propulsion, and, while the motion can be simulated computationally using ad hoc models, there is no comprehensive theoretical paradigm that captures the full range of out-of-equilibrium effects. A variety of experimental and theoretical frameworks have been employed to study micro/nanoswimmer motion in various scenarios (15–23), leading to interesting discoveries about transport behaviors near interfaces. For example, Das et al. found that boundaries could be used to steer self-propelled Janus particles since they tend to move along solid/liquid interfaces (21). Similarly, Brown et al. found that self-propelled Janus particles orbit individual colloids and stochastically hop between neighboring colloids with a hopping rate inversely correlated with fuel concentration when swimming in a two-dimensional colloidal crystal (22).

While previous studies have provided important insights about the effects of interfaces on micro/nanoswimmer transport, the dynamics in complex interface-rich environments remain to be clarified. Since potential applications often involve transport in porous media, where objects must search for and then translocate through narrow pores/openings, technological use of micro- and nanoscale robots will rely on an understanding of how self-propulsion influences transport in a three-dimensional (3D) porous medium, which in turn relies on elementary processes involving narrow hole searching and translocation.

To address this question, we designed and employed an experimental system to quantitatively investigate nanoswimmer transport in porous media and performed comprehensive computational simulations to isolate the effects of individual transport mechanisms. In particular, we used self-propelled Janus particles as model nanoswimmers and highly ordered silica inverse opals as a model porous medium. Using 3D single-particle tracking, we quantitatively investigated the cavity escape process (i.e., the translocation through bottleneck areas between cavities), which is the rate-determining process for transport in many porous environments (24–30). A successful cavity escape consists of two processes: 1) the search for an opening on the cavity and 2) the subsequent translocation through the opening. By directly comparing the motion of nanoswimmers and equivalent passive Brownian particles (31–39),

Significance

As with living microorganisms, many real-world applications of synthetic micro/nanoswimmers are likely to rely on transport in complex environments, a phenomenon that remains poorly understood. Here, we report anomalously rapid transport of self-propelled particles in a porous medium, where nanoswimmers escaped from cavities more than an order of magnitude faster than expected compared to corresponding Brownian particles. This phenomenon was determined to be due to nuanced effects associated with self-propulsion, including enhanced mobility in confinement, efficient surface-mediated searching for holes, and the abolition of barriers at cavity exits. These mechanisms are broadly generalizable, and the previously unknown transport efficiency of nanoswimmers in complex porous environments suggests tremendous opportunities in forward-looking applications, including drug delivery and environmental remediation.

Author contributions: H.W. and D.K.S. designed research; H.W. and B.G. performed research; H.W. and D.K.S. analyzed data; and H.W. and D.K.S. wrote the paper.

The authors declare no competing interest.

This article is a PNAS Direct Submission. M.P.B. is a guest editor invited by the Editorial Board.

[1]To whom correspondence may be addressed. Email: daniel.schwartz@colorado.edu.

This article contains supporting information online at https://www.pnas.org/lookup/suppl/doi:10.1073/pnas.2101807118/-/DCSupplemental.

Published June 28, 2021.

we found that nanoswimmers exhibited significantly (greater than 20×) accelerated cavity escape compared to passive Brownian particles, which was due to a combination of enhanced mobility, efficient searching for holes due to preferential motion along internal cavity surfaces, and self-propelled thrust-enhanced translocation across repulsive barriers to hole escape. In particular, enhanced mobility and surface-mediated searching facilitated the search step, while the additional force due to self-propulsion facilitated the translocation step, converting the cavity escape process from barrier-limited to search-limited.

Results

Tracking Particles in the Porous Medium. As a porous medium, we employed a silica inverse opal film, prepared by evaporative deposition of monodispersed polystyrene colloidal particles from a hydrolyzed silicate sol-gel precursor solution (40). The resulting structure exhibited a hexagonally close-packed interconnected network of spherical cavities, where each cavity had 12 holes connecting to neighboring cavities. The connecting holes allow the confined particle to hop between adjacent cavities and explore the porous structure. As tracer particles, we employed fluorescently labeled platinum–polystyrene Janus particles (hydrodynamic radius of 129 nm), which were dispersed into a glycerol/water mixture (1:1 by weight) at concentrations in the range 10^{-16} to 10^{-15} M. Tracer particles were prepared by dispersing a dilute suspension of carboxylate-modified fluorescent polystyrene beads (Thermo Fisher Scientific) on a glass slide, sputter coating a thin layer of platinum, and subsequently liberating the particles from the glass slide by sonication into pure water. Hydrogen peroxide (3 weight percent [wt%]) was used as chemical fuel to convert the passive Brownian particles into nanoswimmers. When a Janus platinum–polystyrene particle is immersed in an aqueous solution containing hydrogen peroxide, the platinum-coated hemisphere catalyzes the hydrogen peroxide decomposition reaction, while the polystyrene hemisphere remains inert. This asymmetric reaction surrounding the Janus particles generates a concentration gradient, leading to self-propulsion behaviors governed by self-diffusiophoresis (1).

We performed 3D single-particle tracking to directly visualize tracer particle transport within the inverse opal void space (41). The refractive index of the liquid filling the medium was matched to that of the silica framework, and 3D single-particle tracking was enabled by double-helix point spread function imaging using a SPINDLE module (Double Helix Optics, Inc.), where the position in the axial direction was encoded into the shape of the engineered point spread function (42, 43). Conventional two-dimensional (2D) single-particle tracking approaches have been widely used to study the motion of micro/nanoswimmers (19–22, 44–47); however, 3D tracking is necessary to quantitatively study the cavity escape process. In particular, 3D tracking uniquely enables unambiguous identification of all escape events, since 2D projections of 3D trajectories often fail to identify events that involve transitions between cavities whose 2D projections have significant overlap (Fig. 1). Fig. 1 *C* and *E* show representative particle trajectories of a passive Brownian particle and a nanoswimmer within inverse opals, respectively. Fig. 1 *D* and *F* show the corresponding particle coordinates as a function of time for these two types of particles. Qualitatively, passive particles were more likely to explore the full volume of a given cavity, while nanoswimmers tended to move along the internal cavity surface. This behavior is consistent with previous observations of micro/nanoswimmers in the vicinity of planar solid–liquid interfaces (16, 19, 21).

Nanoswimmers Have Enhanced Mobility in Confinement. The mechanisms of transport at various time scales can be visualized using the ensemble-averaged mean squared displacement (MSD) $\Delta r(\tau)^2 = \langle |r(t+\tau) - r(t)|^2 \rangle$, where t represents elapsed time within a trajectory, τ represents the lag time, and r denotes the 3D position. Fig. 2*A* shows plots of MSD versus τ for platinum–polystyrene Janus particles in various solvents. In unconfined liquid, the passive particles exhibited an MSD that was linear in lag time (Fickian diffusion) with a diffusion coefficient of 0.28 ± 0.01 $\mu m^2/s$, and the active nanoswimmers were only slightly superdiffusive, with an apparent diffusion coefficient of 0.47 ± 0.03 $\mu m^2/s$, an approximate 70% enhancement. The uncertainty of the diffusion coefficient was estimated as the SE from multiple independent experiments. While nanoswimmers hypothetically exhibit ballistic motion for short time scales, at times longer than the characteristic rotational diffusion time $\tau_R = \frac{k_B T}{8\pi\eta R^3} = 0.08 \quad s$ (which is smaller than the shortest lag time measured), the propulsion direction was randomized, and an active nanoswimmer exhibited apparent Brownian motion with an enhanced apparent translational diffusion coefficient, $D_{active} = D_{passive} + V^2\tau_R/6$ in 3D space, where V is the propulsion velocity (16).

Compared to motion in the unconfined liquid, both passive Brownian particles and nanoswimmers exhibited slower movement in the porous medium, consistent with the various confinement effects caused by the porous environment. At short times, both passive and active particles in confinement exhibited approximately Fickian behavior, since particles were still exploring the cavity and had not yet experienced the confinement induced by the cavity wall. In this regime, passive particles exhibited an apparent diffusion coefficient $D_{passive} = MSD/(6 \quad \tau) = 0.1 \pm 0.01$ $\mu m^2/s$, and nanoswimmers showed a faster apparent short-time diffusion coefficient, with $D_{active} = 0.3 \pm 0.02$ $\mu m^2/s$. In both cases, this short-time diffusion was inhibited compared to diffusion in unconfined liquid, presumably due to enhanced drag from hydrodynamic effects within cavities. Unexpectedly, this slowing was significantly greater for passive particles (whose diffusion coefficient was 3× smaller in confinement compared to unconfined) than for active nanoswimmers (whose apparent short-time diffusion was reduced by only 35% under confinement). As a result, the short-time diffusion for nanoswimmers, which was only ~70% greater than that of passive particles in unconfined liquid, was 3× greater under confinement. This anomalously high mobility within the geometrically confined void space may be due to enhancement of concentration gradients, which has the potential to intensify self-propulsion effects associated with self-diffusiophoresis. In particular, while conventional hydrodynamic effects associated with geometric confinement (e.g., enhanced drag near walls and recirculation of displaced fluid) are of course expected to inhibit mobility of all particles, the unique self-propulsion mechanisms of nanoswimmers, which depend on concentration gradients, may be enhanced, counteracting the increased drag (15). This anomalously high confined mobility represents one contribution toward the enhanced cavity escape of nanoswimmers relative to Brownian particles.

Over longer time scales in inverse opals, passive Brownian particles exhibited the classic three-regime MSD behavior for "caged" motion. As described above, for lag times shorter than the time required to explore the cavity, the MSD grew linearly with lag time. At intermediate lag times, the MSD plot curved downward, even exhibiting a distinct plateau due to transient trapping within cavities. At long lag times, the MSD gradually increased again as passive Brownian particles escaped out of the confined cavity and hopped among neighboring cavities. This three-regime MSD behavior of passive Brownian particles was qualitatively similar to the caging and jumping behavior observed for a particle confined in a porous medium (48, 49). The MSD of nanoswimmers, on the other hand, gradually evolved from Fickian to modestly subdiffusive motion but did not exhibit distinct caging behavior, qualitatively suggesting efficient searching for holes and rapid translocation.

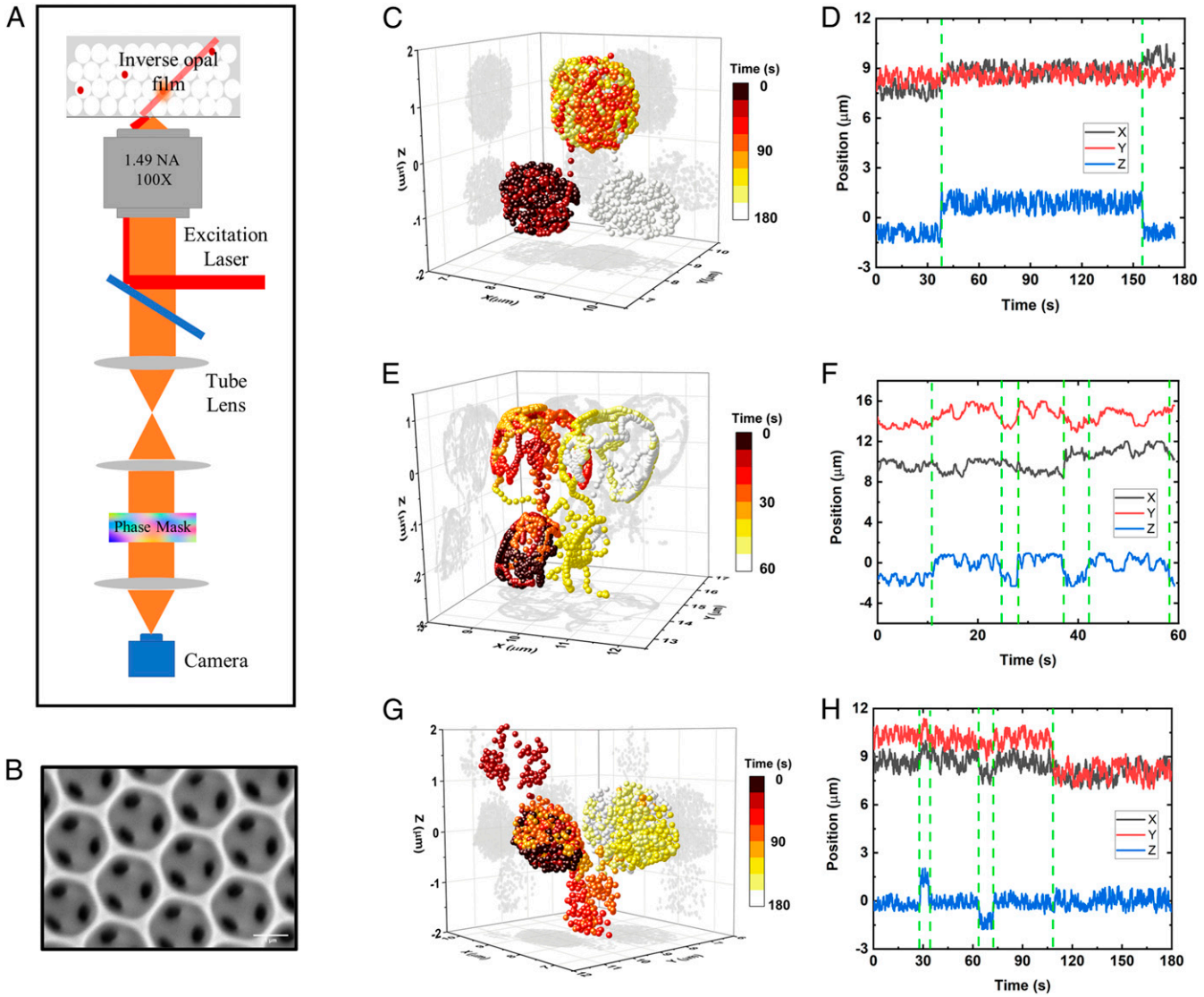

Fig. 1. Experimental schematic and representative trajectories. (*A*) A microscope was equipped with a phase mask and relay optics that enabled double-helix point spread function imaging. (*B*) Representative scanning electron microscope image of an inverse opal film structure (scale bar, 1 μm). (*C*) A representative 3D trajectory of a passive Brownian particle in an inverse opal. (*D*) Corresponding Cartesian coordinates vs. time of a passive Brownian particle in an inverse opal. The vertical dashed lines represent escape events. (*E*) A representative 3D trajectory of an active nanoswimmer in an inverse opal. (*F*) Corresponding Cartesian coordinates vs. time of an active nanoswimmer in an inverse opal. (*G*) A representative 3D trajectory of a passive Brownian particle in an inverse opal with added salt. (*H*) Corresponding particle Cartesian coordinates vs. time of a passive Brownian particle in an inverse opal with added salt. Inverse opals used in these three representative trajectories have 2-μm cavities with 498-nm connecting holes.

Accelerated Cavity Escape of Nanoswimmers. We recently demonstrated an explicit connection between macroscopic long-time diffusion in a porous medium and microscopic pore-level processes (37). In particular, we found that the macroscopic diffusion coefficient can be predicted with a knowledge of cavity escape kinetics and geometrical properties of the medium. The key parameter to characterize cavity escape is the sojourn time, also known as the first passage time through a given cavity. To determine these time intervals, we identified the escape from one cavity to another by monitoring the positional fluctuations in all three dimensions using a maximum allowed displacement algorithm (36). Fig. 1 *D* and *F* show representative results employing this method. By extracting hundreds of sojourn times for each experimental condition, we calculated complementary cumulative distributions of sojourn times in inverse opals for both passive Brownian particles and active nanoswimmers (Fig. 2*B*). We found that the mean sojourn time of a nanoswimmer was more than 20× shorter than that of corresponding passive Brownian particles (Fig. 3*A*). For example, in an inverse opal film with 2-μm diameter cavities and 498-nm holes, the mean sojourn time decreased from 68.2 to 2.8 s after adding chemical fuel to convert passive Brownian particles into nanoswimmers. This suggested that the active motion of nanoswimmers dramatically accelerated the cavity escape process, enhancing transport in porous media. Moreover, at intermediate lag times, the MSD for nanoswimmers curved slightly downward but did not exhibit a distinct plateau like a passive Brownian particle. This suggested that nanoswimmers were weakly confined (i.e., their transport was only slightly influenced by the cavity escape process), which is consistent with their significantly reduced mean sojourn time.

While the threefold enhancement in the short-time mobility contributes to faster searching for holes, it clearly cannot explain the >20× reduction of the mean sojourn time. Moreover, the short-time mobility is not always simply related to the mean

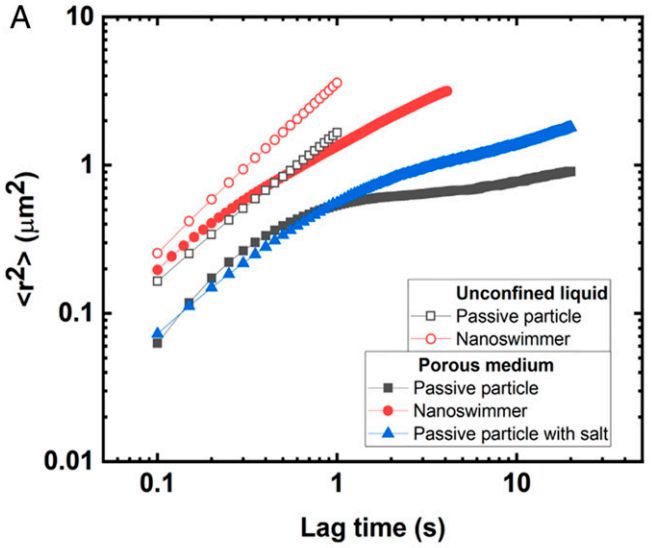

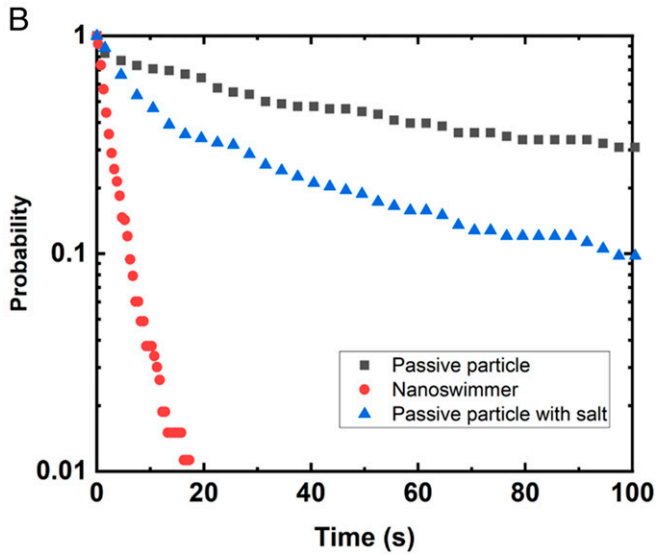

Fig. 2. Statistical analyses of experimental results of Janus platinum–polystyrene particle in various solvent conditions. (*A*) Mean square displacement of catalytic Janus particle under various conditions. A 50 wt% glycerol/water mixture was used as a solvent for passive particles; passive experiments with salt employed 50 wt% glycerol/water with 0.001 M NaCl added. Nanoswimmer experiments employed a 50 wt% glycerol/water mixture with 3 wt% hydrogen peroxide. The porous media used in the experiments were inverse opals with 2-μm diameter cavities and 498-nm connecting holes. The tracer particle radius was 129 nm. (*B*) Complementary cumulative probability distribution of cavity sojourn times under various solution conditions.

sojourn time. Since the cavity escape process involves both search and escape steps, faster diffusion alone does not guarantee a decrease of the sojourn time if it is an escape-limited process. On the other hand, as illustrated by the trajectories in Fig. 1 *C* and *E*, passive Brownian particles and nanoswimmers exhibited qualitatively different search modes. In particular, passive Brownian particles executed 3D searches, typically avoiding the cavity walls, while nanoswimmers tended to move along the walls. The radial position probability distribution provided quantitative confirmation of this observation (Fig. 3*B*). While the detailed mechanisms are not entirely understood, for certain regimes of self-propelled speed and rotational diffusion coefficient, self-propelled particles have been observed to move along solid–liquid interfaces (16, 18, 19, 21). In the current experiments, this leads to a distinctive search process for holes, where nanoswimmers preferentially move along the internal cavity surface. Interestingly, it has been predicted theoretically that related surface-mediated motion can accelerate the search process in the so-called "narrow escape" problem (50, 51). For example, a surface-mediated diffusive search can accelerate the search process more than threefold for a small hole in a circular 2D domain. Therefore, in addition to enhanced mobility, we hypothesized that efficient surface-mediated searching, enabled by a nanoswimmer's tendency to move along boundaries, could accelerate the cavity escape process.

Comparison between Experiments and Simulations. To fully understand the significantly enhanced escape process of nanoswimmers, we performed kinetic Monte Carlo simulations for both passive Brownian particles and nanoswimmers. In these simulations, we created a spherical cavity structure with 12 holes on the surface in a 3D Cartesian coordinate system; a particle was initially placed at the cavity center. In the passive Brownian particle scenario, the

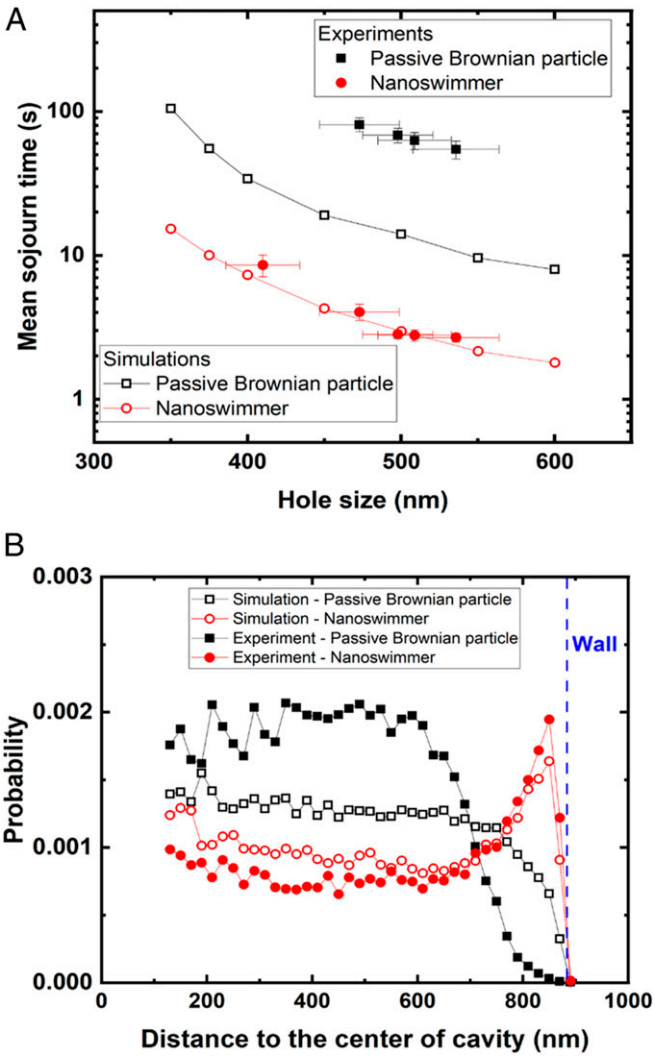

Fig. 3. Comparison of experiments and kinetic Monte Carlo simulations. (*A*) Mean sojourn time versus hole size. The uncertainty of the hole size represents the SD of the hole size measurements from SEM images. The uncertainty of the mean sojourn time represents the SE of the sojourn time measurements. (*B*) Radial position probability distribution of confined particle in inverse opal cavity.

particle motion was modeled as Brownian motion with the short-time diffusion coefficient obtained from experiments (thereby incorporating hydrodynamic effects empirically). In the nanoswimmer scenario, the nanoswimmer motion was modeled as the combined action of random translational and rotational diffusion processes and directed self-propulsion (52). In particular, the self-propulsion effects were simulated as a motion with constant directional speed, where the direction depends on the particle orientation, which undergoes rotational diffusion. The simulation details are described in *SI Appendix*.

Nanoswimmer simulations showed that self-propelled motion resulted in an enhanced probability of the particle being near the internal wall of the spherical cavity, consistent with the experimental observations. In contrast, both experimental data and simulations of passive Brownian particles exhibited depletion near the cavity wall. For simulated particles, this depletion was presumably due to steric effects, with the length scale dominated by the particle size. However, the depletion region obtained from experimental observations of passive Brownian particles was significantly more extended, suggesting long-range repulsion from cavity walls (Fig. 3*B*), consistent with previous findings (35, 36, 41). In particular, electrostatic repulsion between cavity walls and passive Brownian particles can inhibit the cavity escape process and decrease the effective hole size, leading to a barrier-limited escape process. Importantly, we found that nanoswimmer simulations were in good quantitative agreement with experimental nanoswimmer mean sojourn times but that Brownian simulations underestimated the respective mean sojourn times (Fig. 3*A*) by ~5×. This comparison suggested that nanoswimmer escape was search-limited, but Brownian passive escape was barrier-limited.

Based on these observations, we hypothesized that the significantly enhanced cavity escape process of nanoswimmers relative to corresponding passive Brownian particles was due to the combination of three effects: 1) enhanced short-time mobility, 2) an efficient surface-mediated search mechanism, and 3) effective abolition of barriers at hole exits, which converted the cavity escape process of nanoswimmers to search-limited from barrier-limited. As described below, a combination of control experiments and kinetic Monte Carlo simulations allowed us to isolate and quantify the effects of these three mechanisms.

Efficient Searching for Holes along Cavity Surfaces. The effects of enhanced mobility and surface-mediated searching were decoupled by modeling the cavity escape process of a passive Brownian particle with different translational diffusion coefficients and boundary conditions (*SI Appendix*, Fig. S6). In particular, reflective boundary conditions at the cavity walls were used to mimic the 3D searching behavior of passive particles, while an adsorptive boundary condition was used to mimic the 2D surface searching behavior of nanoswimmers (i.e., after a pseudonanoswimmer first encountered a wall, it subsequently diffused along the interior cavity surface). Experimentally measured short-time diffusion coefficients of passive particle and nanoswimmers were used to represent the respective short-time mobilities.

These individual effects are visualized in Fig. 4*A*, which uses passive particles with reflective boundary conditions (3D searching) as a baseline and graphs the reduction of search time associated with 1) faster effective short-time mobility due to self-propulsion, 2) surface-mediated (2D) searching without enhanced mobility, and 3) both effects combined. Interestingly, surface-mediated searching significantly accelerated the escape process in the small hole size regime, while the impact of faster short-time mobility increased with increasing hole size. For the specific hole size (498 nm) employed in the experiments, each effect contributed approximately equally to the reduction in search time, for a total enhancement of ~5× compared to the experimentally measured nearly 25× enhancement of mean sojourn time.

Interestingly, the simulated sojourn times that were based on simplified Monte Carlo simulations of passive Brownian motion with qualitative nanoswimmer transport features (i.e., enhanced short-time mobility and surface-mediated search) were in reasonably good agreement with the experimental measured values for the nanoswimmer (Fig. 4*B*). This agreement further confirms the importance of the combined effects of enhanced mobility and surface-mediated searching in facilitating the cavity escape process, in that simply incorporating qualitative transport features of nanoswimmers into passive Brownian particle simulations provided a fairly accurate approximation of mean sojourn times. The full-featured nanoswimmer simulations predicted the experimentally measured value with better accuracy over the full range of hole sizes. A significant difference between these two types of simulations involved the assumption of purely 2D surface diffusion in the simplified passive Brownian particle simulation, which overestimated the escape rate in the small hole size regime while underestimating the escape rate in the large hole size regime.

Self-Propulsion Overcomes Repulsive Barriers to Cavity Escape. We hypothesized that the discrepancy between the experimentally observed mean sojourn time of passive particles (68.2 s) and the predicted value from simulations (14 s) was due to a reduction in the effective hole size caused by electrostatic repulsion at walls and hole exits (as suggested in Fig. 3*B*), since the carboxylate-modified particles and silica framework are both negatively charged. Previous studies showed that like-charge electrostatic interactions can inhibit cavity escape by forming energy barriers at hole exits. This can be modeled as a reduction in the apparent hole size. Added salt can screen this repulsion, increasing the effective hole size and accelerating cavity escape (36). Therefore, we performed additional experiments using the same passive particles and porous medium with 0.001 M sodium chloride added, and, as expected, the mean sojourn time was reduced from 68.2 to 32.5 s (Fig. 2*B*). Fig. 1*G* shows a representative trajectory obtained under these conditions; it is qualitatively similar to a Brownian trajectory in the absence of salt in that the confined particle explored the 3D volume of the cavity. However, the MSD plot (Fig. 2*A*) in the presence of salt exhibits less confinement at intermediate times, consistent with facilitated hole translocation that led to faster escape to adjacent cavities. However, as illustrated in Fig. 4*C*, even in the presence of salt, the cavity escape was still slower than predicted by 3D simulations, suggesting the remaining presence of a small barrier to escape.

To understand this effect more quantitatively, the effective hole size was calculated using a potential energy profile model developed by Bowen et al. (53, 54), which was based on Derjaguin-Landau-Verwey-Overbeek (DLVO) theory and included both electrostatic and van der Waals interactions. The effective hole was taken to be the region where the potential energy was less than k_BT, and the calculation details are described in *SI Appendix*. The effective hole sizes for a physical hole of 498 nm were calculated to be 368 and 416 nm in the absence of salt and the presence of 0.001 M salt, respectively. Consistent with our previous findings, the discrepancies between experimental and simulated sojourn times were successfully explained by calculating effective hole sizes associated with electrostatic energy barriers (Fig. 4*C*).

Interestingly, the simulated mean sojourn time of a surface-searching nanoswimmer for an equivalent effective hole size (368 nm) was calculated to be ~8 s, which was more than 2× the measured sojourn time of 2.8 s. Additional experiments performed with different hole sizes showed similar discrepancies (*SI Appendix*, Fig. S7). These findings, combined with the agreement between simulated and experimental nanoswimmer sojourn times in the absence of salt, suggested that the active nanoswimmers were not significantly affected by electrostatic barriers at hole exits despite the like charge repulsion that clearly limits

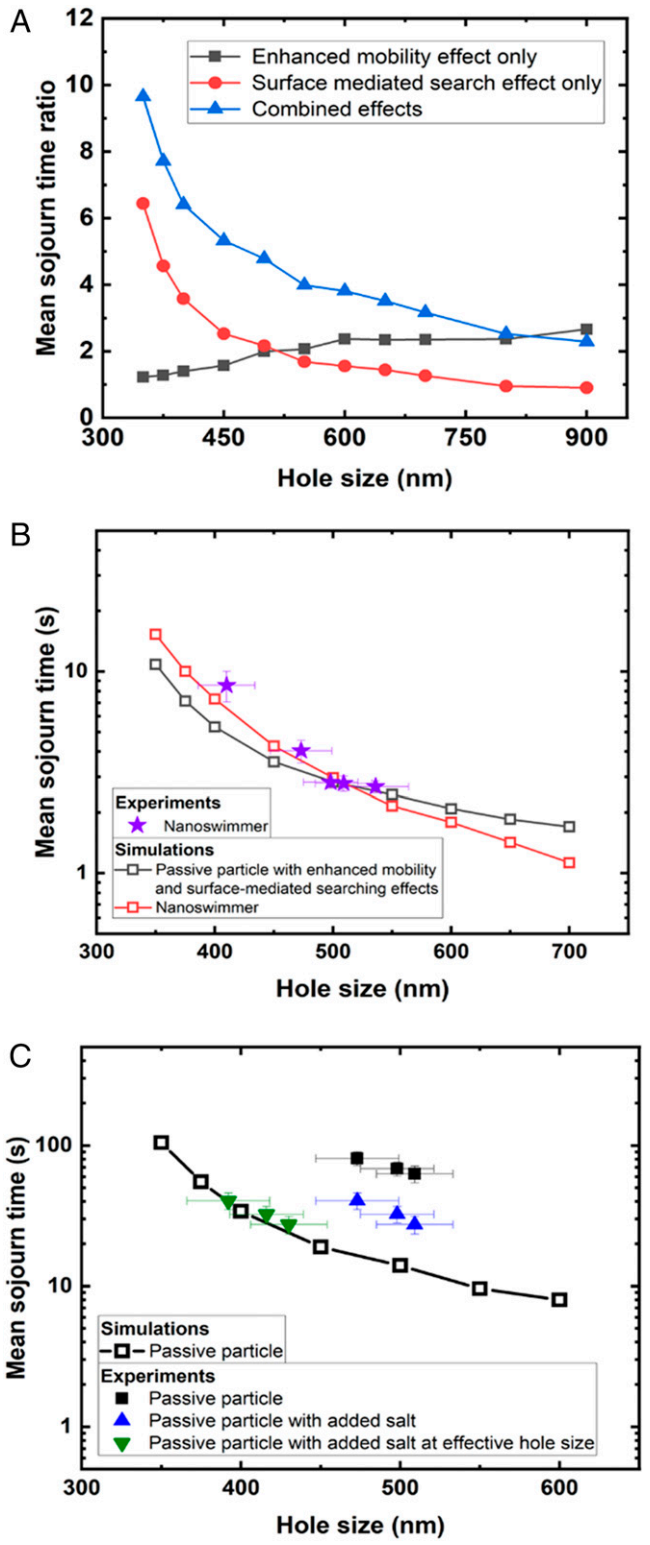

Fig. 4. Effects of enhanced mobility, surface-mediated searching, and barrier elimination on mean sojourn times. (*A*) Mean sojourn time ratio as a function of hole size, showing the decoupled effects of enhanced mobility and surface-mediated searching. (*B*) Comparison of experimental nanoswimmer observations with two types of Monte Carlo simulations: an explicit nanoswimmer simulation and a passive Brownian simulation with nanoswimmer features. (*C*) Comparison of passive Brownian particle simulations with experimental observations of passive Brownian particles with added salt. The green inverted triangles represent the same added-salt experimental data but with effective hole sizes calculated based on an electrostatic model as described in the text.

the escape of the same particles in the absence of fuel. We hypothesized that self-propulsion provides forces that can overcome repulsion, leading to an escape process for nanoswimmers that is entirely search limited, with no additional effect due to barriers to translocation. To test the plausibility of this hypothesis, we compared the self-propulsion force to the barrier force due to electrostatic repulsion. The self-propulsion force was estimated using the Stokes equation $F_p = 6\pi\mu RV = 55$ fN, and the barrier force was calculated based on Bowen's model (53), where the largest barrier force in the presence of 0.001 M salt was ~35 fN (*SI Appendix*, Fig. S3*C*). This comparison provides a consistency check, suggesting that self-propulsion can provide additional forces of the same order of magnitude as typical electrostatic repulsion, thereby allowing confined nanoswimmers to overcome the barrier at hole exits, converting the cavity escape process from a barrier-limited to a search-limited process.

Mechanisms of Accelerated Nanoswimmer Cavity Escape. Overall, the accelerated cavity escape of nanoswimmers, compared to Brownian particles in the absence of chemical fuel, was due to the combined effects of an enhanced short-time mobility, surface-mediated searching, and the effective abolition of repulsive barriers at hole exits. In particular, the negation of repulsive barriers due to self-propulsion force facilitated the translocation step, converting the barrier-limited process to search-limited; enhanced short-time mobility and efficient surface-mediated searching facilitated the search step. Taking the hole size of 498 nm as a representative example, the mean sojourn time of nanoswimmer was nearly 25× shorter than that of a passive Brownian particle in salt-free glycerol/water solvent (Fig. 5). Breaking down this enhancement factor, the negation of repulsive barriers reduced the mean sojourn time fivefold, and the combined effects of enhanced diffusion and surface-mediated searching also reduced the mean sojourn time by fivefold.

Discussion

The rate-determining process for the transport of particles or macromolecules in porous media involves translocation through pore constrictions. Here, we quantitatively studied the cavity escape of passive Brownian particles and nanoswimmers using a well-defined system enabled by 3D single-particle tracking. We found that nanoswimmers escaped from cavities more than an order of magnitude faster than expected relative to passive Brownian particles, despite the fact that their mobility in unconfined liquid was less than twofold faster. This anomalously rapid rate of escape suggests that micro/nanoswimmers have tremendous transport efficiency in complex and tortuous environments, which are broadly relevant to biomedical and environmental applications.

The fundamental difference between a micro/nanoswimmer and its corresponding passive Brownian particle is self-propulsion, which is naïvely characterized by speed. However, we found that self-propulsion induces additional nuanced effects whose impacts are dramatically amplified in complex environments, leading to extremely rapid cavity escape. In particular, the slowing effects of hydrodynamic drag in a confined environment were mitigated compared to a Brownian passive particle, resulting in anomalously fast short-time mobility. Moreover, self-propulsion resulted in qualitatively different phenomena, such as surface-mediated searching and the abolition of energy barriers at hole exits. The results reported here provide a comprehensive picture of the mechanisms that enhance micro/nanoswimmer transport in confined and porous media and also hint at the immense potential of micro/nanoswimmers in biomedical and environmental applications. For example, low–ionic strength conditions are often necessary in various technological applications to prevent aggregation and surface adsorption via electrostatic repulsion (55–57). However, these conditions have undesirable side effects, such as anomalously slow transport in porous materials. Our findings

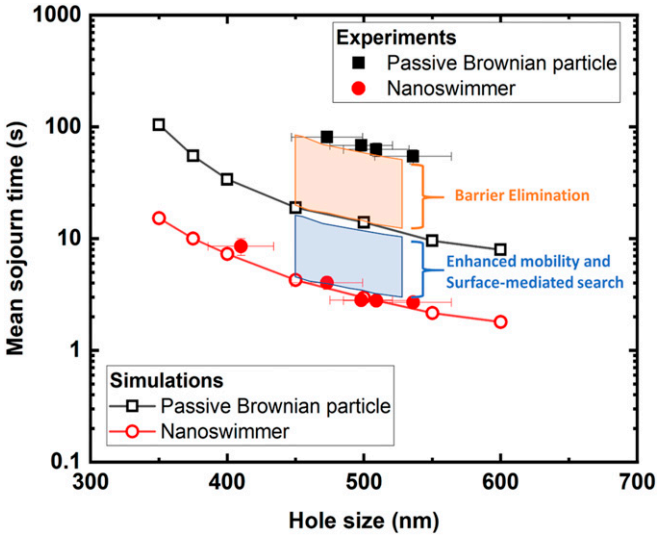

Fig. 5. Mechanisms of accelerated nanoswimmer cavity escape.

suggest that micro/nanoswimmers can effectively address these undesirable side effects through self-propulsion.

It is interesting to consider how the phenomena observed here might apply to biological microswimmers. Such a comparison must distinguish between "pusher" and "puller" type microbes. Since "pusher" type microbes hydrodynamically attracted to solid surfaces, the searching process for exit holes may be enhanced because of efficient surface-mediated searching, while "puller" type microbes may exhibit longer search times since they are hydrodynamically repelled from solid surfaces (58–60). Therefore, compared to "pusher" type microbes, the transport of "puller" type microbes in porous media is expected to be inhibited.

Materials and Methods

Preparation of Silica Inverse Opals. Silica inverse opals were prepared by evaporative deposition of monodispersed polystyrene beads from a hydrolyzed silicate sol-gel precursor solution. Specifically, 0.25 mL 5 vol% monodispersed colloidal polystyrene suspension (2 μm in diameter) was added to 9.75 mL Milli-Q water and 30 to 100 μL hydrolyzed tetraethyl orthosilicate (TEOS) solution. The cavity size was determined by the size of colloidal polystyrene beads, while the hole size was determined by the concentration of TEOS solution. A standard TEOS solution consisted of anhydrous ethanol, tetraethoxysilane, and 0.10 M hydrogen chloride at a volume ratio of 1:5:1:1. The standard TEOS solution was stirred for 1 h at room temperature prior to use. A 25-mm diameter microscope glass slide was used as a substrate; it was vertically suspended in a beaker containing the colloidal polystyrene beads and standard TEOS solution. The solution was evaporated in a 70 °C oven for 2 d to form a thin film of opal structure on the glass slide. The resulting opal film was then pyrolyzed in a furnace at 500 °C for 2 h to remove the templating polystyrene particles and form a silica inverse opal film.

Imaging Nanoparticle Diffusion in Inverse Opals. A Nikon N-STORM super-resolution microscope equipped with a phase mask was used for single-particle tracking experiments. 3D tracking was enabled by a SPINDLE module including a phase mask and a filter (Double Helix Optics, Inc.), which transformed the standard point spread function to a double-helix point spread function, where the position in the Z direction was encoded into the shape of double-helix point spread function. Approximately 50 movies per sample were captured at different spatial locations within the silica inverse opal samples. DH-TRAXTM tracking software was used to identify the particle position, with precisions of 10 nm laterally and 20 nm axially.

Data Availability. All study data are included in the article and/or *SI Appendix*, and full-length raw movies are available upon request.

ACKNOWLEDGMENTS. This work was supported by the US Department of Energy, Office of Science, Basic Energy Sciences, under Award No. DE-SC0001854.

1. J. R. Howse *et al.*, Self-motile colloidal particles: From directed propulsion to random walk. *Phys. Rev. Lett.* **99**, 048102 (2007).
2. S. Wang, N. Wu, Selecting the swimming mechanisms of colloidal particles: Bubble propulsion versus self-diffusiophoresis. *Langmuir* **30**, 3477–3486 (2014).
3. W. Gao, S. Sattayasamitsathit, K. M. Manesh, D. Weihs, J. Wang, Magnetically powered flexible metal nanowire motors. *J. Am. Chem. Soc.* **132**, 14403–14405 (2010).
4. S. Tottori *et al.*, Magnetic helical micromachines: Fabrication, controlled swimming, and cargo transport. *Adv. Mater.* **24**, 811–816 (2012).
5. J. Wang *et al.*, A silicon nanowire as a spectrally tunable light-driven nanomotor. *Adv. Mater.* **29**, 1701451 (2017).
6. R. Dong, Y. Cai, Y. Yang, W. Gao, B. Ren, Photocatalytic micro/nanomotors: From construction to applications. *Acc. Chem. Res.* **51**, 1940–1947 (2018).
7. W. Wang, L. A. Castro, M. Hoyos, T. E. Mallouk, Autonomous motion of metallic microrods propelled by ultrasound. *ACS Nano* **6**, 6122–6132 (2012).
8. L. Ren, W. Wang, T. E. Mallouk, Two forces are better than one: Combining chemical and acoustic propulsion for enhanced micromotor functionality. *Acc. Chem. Res.* **51**, 1948–1956 (2018).
9. W. Duan *et al.*, Synthetic nano- and micromachines in analytical chemistry: Sensing, migration, capture, delivery, and separation. *Annu. Rev. Anal. Chem. (Palo Alto, Calif.)* **8**, 311–333 (2015).
10. F. Soto, J. Wang, R. Ahmed, U. Demirci, Medical micro/nanorobots in precision medicine. *Adv. Sci. (Weinh.)* **7**, 2002203 (2020).
11. J. Li, B. Esteban-Fernández de Ávila, W. Gao, L. Zhang, J. Wang, Micro/nanorobots for biomedicine: Delivery, surgery, sensing, and detoxification. *Sci. Robot.* **2**, eaam6431 (2017).
12. J. R. Baylis *et al.*, Self-propelled particles that transport cargo through flowing blood and halt hemorrhage. *Sci. Adv.* **1**, e1500379 (2015).
13. W. Gao, J. Wang, The environmental impact of micro/nanomachines: A review. *ACS Nano* **8**, 3170–3180 (2014).
14. L. Soler, V. Magdanz, V. M. Fomin, S. Sanchez, O. G. Schmidt, Self-propelled micromotors for cleaning polluted water. *ACS Nano* **7**, 9611–9620 (2013).
15. F. Yang, S. Qian, Y. Zhao, R. Qiao, Self-diffusiophoresis of Janus catalytic micromotors in confined geometries. *Langmuir* **32**, 5580–5592 (2016).
16. C. Bechinger *et al.*, Active particles in complex and crowded environments. *Rev. Mod. Phys.* **88**, 045006 (2016).
17. R. Alonso-Matilla, B. Chakrabarti, D. Saintillan, Transport and dispersion of active particles in periodic porous media. *Phys. Rev. Fluids* **4**, 043101 (2019).
18. G. Volpe, I. Buttinoni, D. Vogt, H.-J. Kümmerer, C. Bechinger, Microswimmers in patterned environments. *Soft Matter* **7**, 8810–8815 (2011).
19. J. Simmchen *et al.*, Topographical pathways guide chemical microswimmers. *Nat. Commun.* **7**, 10598 (2016).
20. T. Bhattacharjee, S. S. Datta, Bacterial hopping and trapping in porous media. *Nat. Commun.* **10**, 2075 (2019).
21. S. Das *et al.*, Boundaries can steer active Janus spheres. *Nat. Commun.* **6**, 8999 (2015).
22. A. T. Brown *et al.*, Swimming in a crystal. *Soft Matter* **12**, 131–140 (2016).
23. H. R. Jiang, N. Yoshinaga, M. Sano, Active motion of a Janus particle by self-thermophoresis in a defocused laser beam. *Phys. Rev. Lett.* **105**, 268302 (2010).
24. R. A. Siegel, R. Langer, A new Monte-Carlo approach to diffusion in constricted porous geometries. *J. Colloid Interface Sci.* **109**, 426–440 (1986).
25. W. M. Saltzman, R. Langer, Transport rates of proteins in porous materials with known microgeometry. *Biophys. J.* **55**, 163–171 (1989).
26. R. A. Siegel, J. Kost, R. Langer, Mechanistic studies of macromolecular drug release from macroporous polymers. 1. Experiments and preliminary theory concerning completeness of drug release. *J. Control. Release* **8**, 223–236 (1989).
27. R. A. Siegel, R. Langer, Mechanistic studies of macromolecular drug release from macroporous polymers. 2. Models for the slow kinetics of drug release. *J. Control. Release* **14**, 153–167 (1990).
28. M. J. Skaug, D. K. Schwartz, Tracking nanoparticle diffusion in porous filtration media. *Ind. Eng. Chem. Res.* **54**, 4414–4419 (2015).
29. M. J. Skaug, L. Wang, Y. Ding, D. K. Schwartz, Hindered nanoparticle diffusion and void accessibility in a three-dimensional porous medium. *ACS Nano* **9**, 2148–2156 (2015).
30. T. Kanti Sen, K. C. Khilar, Review on subsurface colloids and colloid-associated contaminant transport in saturated porous media. *Adv. Colloid Interface Sci.* **119**, 71–96 (2006).
31. O. Bénichou, R. Voituriez, Narrow-escape time problem: Time needed for a particle to exit a confining domain through a small window. *Phys. Rev. Lett.* **100**, 168105 (2008).
32. A. F. Cheviakov, M. J. Ward, R. Straube, An asymptotic analysis of the mean first passage time for narrow escape problems: Part I: The Sphere. *Multiscale Model. Simul.* **8**, 836–870 (2010).
33. Z. Schuss, A. Singer, D. Holcman, The narrow escape problem for diffusion in cellular microdomains. *Proc. Natl. Acad. Sci. U.S.A.* **104**, 16098–16103 (2007).
34. D. S. Grebenkov, R. Metzler, G. Oshanin, Strong defocusing of molecular reaction times results from an interplay of geometry and reaction control. *Commun. Chem.* **1**, 96 (2018).
35. D. Wang, H. Wu, L. Liu, J. Chen, D. K. Schwartz, Diffusive escape of a nanoparticle from a porous cavity. *Phys. Rev. Lett.* **123**, 118002 (2019).

36. H. Wu, R. Sarfati, D. Wang, D. K. Schwartz, Electrostatic barriers to nanoparticle accessibility of a porous matrix. *J. Am. Chem. Soc.* **142**, 4696–4704 (2020).
37. H. Wu, D. Wang, D. K. Schwartz, Connecting hindered transport in porous media across length scales: From single-pore to macroscopic. *J. Phys. Chem. Lett.* **11**, 8825–8831 (2020).
38. D. Nykypanchuk, H. H. Strey, D. A. Hoagland, Brownian motion of DNA confined within a two-dimensional array. *Science* **297**, 987–990 (2002).
39. D. S. Grebenkov, R. Metzler, G. Oshanin, Full distribution of first exit times in the narrow escape problem. *New J. Phys.* **21**, 122001 (2019).
40. B. Hatton, L. Mishchenko, S. Davis, K. H. Sandhage, J. Aizenberg, Assembly of large-area, highly ordered, crack-free inverse opal films. *Proc. Natl. Acad. Sci. U.S.A.* **107**, 10354–10359 (2010).
41. H. Wu, D. K. Schwartz, Nanoparticle tracking to probe transport in porous media. *Acc. Chem. Res.* **53**, 2130–2139 (2020).
42. D. P. Wang, A. Agrawal, R. Piestun, D. K. Schwartz, Enhanced information content for three-dimensional localization and tracking using the double-helix point spread function with variable-angle illumination epifluorescence microscopy. *Appl. Phys. Lett.* **110**, 211107 (2017).
43. S. R. Pavani *et al*., Three-dimensional, single-molecule fluorescence imaging beyond the diffraction limit by using a double-helix point spread function. *Proc. Natl. Acad. Sci. U.S.A.* **106**, 2995–2999 (2009).
44. G. Dunderdale, S. Ebbens, P. Fairclough, J. Howse, Importance of particle tracking and calculating the mean-squared displacement in distinguishing nanopropulsion from other processes. *Langmuir* **28**, 10997–11006 (2012).
45. S. Ebbens, M. H. Tu, J. R. Howse, R. Golestanian, Size dependence of the propulsion velocity for catalytic Janus-sphere swimmers. *Phys. Rev. E Stat. Nonlin. Soft Matter Phys.* **85**, 020401 (2012).
46. T. Bhattacharjee, S. S. Datta, Confinement and activity regulate bacterial motion in porous media. *Soft Matter* **15**, 9920–9930 (2019).
47. A. I. Campbell, S. J. Ebbens, Gravitaxis in spherical Janus swimming devices. *Langmuir* **29**, 14066–14073 (2013).
48. P. M. Reis, R. A. Ingale, M. D. Shattuck, Caging dynamics in a granular fluid. *Phys. Rev. Lett.* **98**, 188301 (2007).
49. I. Y. Wong *et al*., Anomalous diffusion probes microstructure dynamics of entangled F-actin networks. *Phys. Rev. Lett.* **92**, 178101 (2004).
50. O. Bénichou, D. Grebenkov, P. Levitz, C. Loverdo, R. Voituriez, Optimal reaction time for surface-mediated diffusion. *Phys. Rev. Lett.* **105**, 150606 (2010).
51. T. Calandre, O. Bénichou, R. Voituriez, Accelerating search kinetics by following boundaries. *Phys. Rev. Lett.* **112**, 230601 (2014).
52. G. Volpe, S. Gigan, G. Volpe, Simulation of the active Brownian motion of a microswimmer. *Am. J. Phys.* **82**, 659–664 (2014).
53. W. R. Bowen, A. N. Filippov, A. O. Sharif, V. M. Starov, A model of the interaction between a charged particle and a pore in a charged membrane surface. *Adv. Colloid Interface Sci.* **81**, 35–72 (1999).
54. M. M. Kim, A. L. Zydney, Effect of electrostatic, hydrodynamic, and Brownian forces on particle trajectories and sieving in normal flow filtration. *J. Colloid Interface Sci.* **269**, 425–431 (2004).
55. S. Dominguez-Medina, J. Blankenburg, J. Olson, C. F. Landes, S. Link, Adsorption of a protein monolayer via hydrophobic interactions prevents nanoparticle aggregation under Harsh environmental conditions. *ACS Sustain. Chem.& Eng.* **1**, 833–842 (2013).
56. T. L. Moore *et al*., Nanoparticle colloidal stability in cell culture media and impact on cellular interactions. *Chem. Soc. Rev.* **44**, 6287–6305 (2015).
57. W. Zhang, Nanoparticle aggregation: Principles and modeling. *Adv. Exp. Med. Biol.* **811**, 19–43 (2014).
58. E. Lauga, Bacterial hydrodynamics. *Annu. Rev. Fluid Mech.* **48**, 105–130 (2016).
59. K.-T. Wu, Y.-T. Hsiao, W.-Y. Woon, Entrapment of pusher and puller bacteria near a solid surface. *Phys. Rev. E* **98**, 052407 (2018).
60. A. V. Singh *et al*., Mechanical coupling of puller and pusher active microswimmers influences motility. *Langmuir* **36**, 5435–5443 (2020).